Biosensors and Bioelectronics: X 14 (2023) 100328

Contents lists available at ScienceDirect

Biosensors and Bioelectronics: X

journal homepage: www.journals.elsevier.com/biosensors-and-bioelectronics-x

In-vivo measurement of radio frequency electric fields in mice brain

Omid Yaghmazadeh [a,**], Seth Schoenhardt [d], Arya Sarabandi [d], Ali Sabet [d], Kazem Sabet [d], Fatemeh Safari [b], Leeor Alon [b,***], György Buzsáki [a,c,*]

[a] Neuroscience Institute, School of Medicine, New York University, New York, NY, 10016, USA
[b] Department of Radiology, and School of Medicine, New York University, New York, NY, 10016, USA
[c] Department of Neurology, School of Medicine, New York University, New York, NY, 10016, USA
[d] EMAG Technologies Inc., 775 Technology Dr., Ann Arbor, MI, 48108, USA

ARTICLE INFO

Keywords:
Radio frequency
Electric field
Dosimetry
BSO crystal
Electrooptic probe
Environmental health

ABSTRACT

With the development of novel technologies, radio frequency (RF) energy exposure is expanding at various wavelengths and power levels. These developments necessitate updated approaches of RF measurements in complex environments, particularly in live biological tissue. Accurate dosimetry of the absorbed RF electric fields (E-Fields) by the live tissue is the keystone of environmental health considerations for this type of ever-growing non-ionizing radiation energy. In this study, we introduce a technique for direct in-vivo measurement of electric fields in living tissue. Proof of principle in-vivo electric field measurements were conducted in rodent brains using Bismuth Silicon Oxide (BSO) crystals exposed to varying levels of RF energy. Electric field measurements were calibrated and verified using in-vivo temperature measurements using optical temperature fibers alongside electromagnetic field simulations of a transverse electromagnetic (TEM) cell.

1. Introduction

Since the primary Radio Frequency (RF) applications in the early 20th century, the interaction of RF energy with biological tissue and its potential risks have gained a great deal of interest (Daily, 1943; Follis, 1946; Michaelson and Lin, 1987; Vöröslakos et al., 2022). With advancement of novel technologies, the exposure to radio frequency (RF) energy has never stopped expanding. The extent of RF applications and the increase in applied frequencies have resurrected questions with regards to RF energy exposure and its impact on humans (Karipidis et al., 2021). For example, development of high power microwave (HPM) applications for civil and military purposes has generated a new wave of concerns for health implication of RF energy radiation on the brain and the body (Dagro et al., 2021; Foster, 2000). In line with such concerns, the International Commission on Non-Ionizing Radiation Protection (ICNIRP) has recently updated their guidelines for RF energy exposure limits (Ziegelberger et al., 2020).

Studying the effects of RF energy on biological tissue would require methods to accurately measure the absorbed RF energy in the tissue for which the widely used standard parameter is the specific absorption rate (SAR) (Ziegelberger et al., 2020). For example, assessment of the induced RF energy inside biological tissue is essential in various medical interventions (such as Magnetic Resonance Imaging, RF ablation, etc.). Furthermore, it is the core element for studying safety measures related to any RF energy exposures (such as cell phone usage, HPM applications, etc.). SAR and electric field (E-field) can be calculated either experimentally or by numerical simulations. Evidently, experimental assessments are preferable as numerical simulations are often vulnerable to errors in various ways. Due to the complexity of biological systems and the limitations of the E-field probes, it is difficult to conduct measurements in vivo, and as a result, RF compliance measurements are conducted in phantoms that simulate human tissue. However, those compliance measurements may not faithfully reflect real-life scenarios of exposure. Furthermore, many groups are using electromagnetic (EM) field simulations to assess exposure from various devices, but real-life complexities of the environment and tissue anatomy seldom can be replicated in-silico. Both EM field simulations and phantom compliance tests rely on tabulated dielectric properties of tissues measured in euthanized sheep (Gabriel and Gabriel, 1996). However, it is well known that, in live tissue, the physiological variation can greatly impact

* Corresponding author. Neuroscience Institute, School of Medicine, New York University, New York, NY, 10016, USA.
** Corresponding author.
*** Corresponding author.
E-mail addresses: omid.yaghmazadeh@gmail.com (O. Yaghmazadeh), leeor.alon@nyulangone.org (L. Alon), gyorgy.buzsaki@nyulangone.org (G. Buzsáki).

https://doi.org/10.1016/j.biosx.2023.100328
Received 18 October 2022; Received in revised form 10 February 2023; Accepted 5 March 2023
Available online 11 March 2023

those dielectric properties (e.g., water content and hydration), thus reliance on these values may introduce non-negligible errors in RF exposure estimation.

From the materials point of view, the biological tissue constitutes very complex structures with variable composition across different subjects. Although their physical properties have been subject to extensive studies (Gabriel et al., 1996), providing several numerical or phantom representatives, their complexity requires direct experimental measurements for accurate evaluation of any value of interest. Therefore, different biological tissues should be considered as a stand-alone complex material and be examined accordingly, especially when accurate measurements are demanded.

Experimental measurement of in-situ E-fields in biological tissue (or phantom preparations with similar physical properties) induced by RF energy exposure can be performed either by temperature measurements (Schuderer et al., 2004) or using E-field probes (Faraone et al., 2000). Using temperature measurements to assess the in situ E-field is reliable but only for RF energy exposure levels that induce a sufficient temperature rise in the tissue. E-field probes are usually constructed in two ways: metal based (Faraone et al., 2000) or electro-optic (EO) probes (Cecelja and Balachandran, 1999). EO E-field probes have several advantages, such as their non-metallic nature (which makes them minimally invasive to the E-field distribution), wide bandwidth (from DC to several THz (Wu, 1997; Keiber et al., 2016),), very high (pico-sec) temporal resolution (Sulzer et al., 2020), and relatively small dimensions, making them ideal for in vivo measurement. For example, recently developed HPM applications apply very short (μsec range) and very high power (KW/cm^2 to MW/cm^2) RF pulses (Dagro et al., 2021). Measuring the in-situ E-field in biological tissue exposed to such radiation requires both high measuring range and high temporal resolution.

The possibility of direct measurement of induced RF E-fields inside the tissue (either *in-vivo* or *ex-vivo*) provides a more accurate assessment of the in-situ E-Field in living species exposed to such radiation. While E-field measurement in ex-vivo and phantom preparations provide a good insight into the amount of absorbed energy due to RF exposure, in-vivo measurements provide a direct and more accurate evaluation. In this study we introduce a methodology for direct measurement of RF E-fields in mice brain in-vivo where E-field measurements were calibrated and validated by temperature measurements conducted by optical temperature fibers alongside electromagnetic field simulations in a transverse electromagnetic (TEM) cell.

2. Results

We performed in-situ E-field measurements in the brain of head-fixed anesthetized mice exposed to RF energy radiation using a BSO crystal EO E-field probe.

2.1. Electro-Optical E-field measurement system

RF E-field measurements were performed by a commercially available System (NeoScan, EMAG Technologies Inc.). Fig. 1 shows the schematics and photo of the electro-optic field probe and the E-field measurement system. The E-field probe consists of an electro-optic crystal which is cut along one of its optical axes and mounted at the tip of an optical fiber via a graded index (GRIN) lens. The EO probe is mounted either on a fixed stand or on a computer-controlled translation stage and is then immersed in the E-field of the device under test (DUT; Fig. 1B). A continuous wave (CW) laser beam propagating through the optical fiber and then into the EO crystal experiences the Pockels effect, whereby the external E-field penetrating the EO crystal induces a change in its refractive index. As result, the polarization vector of the optical beam is rotated by an angle that is directly proportional to the strength of the E-field (Sarabandi et al., 2017). The change in the polarization state, in turn, produces a measurable change in the optical intensity of the beam as it passes through a polarization analyzer. Finally, a

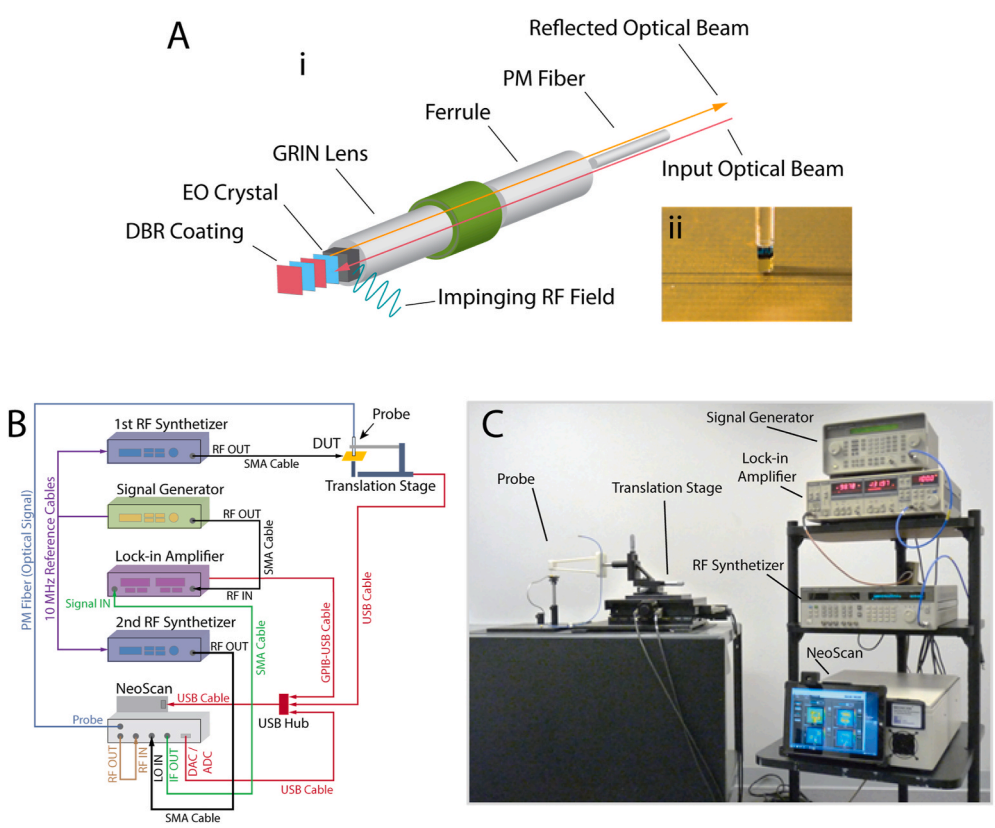

Fig. 1. Electro-Optical E-field measurement system and its principal components. A) 3D drawing (i) and close-up photo (ii) of the 'non-metallic' electro-optic field probe. **B)** Schematic of the E-field measurement system. **C)** Photo of a NeoScan E-field measurement setup.

high-speed photodetector at the end of the optical bench transduces the intensity of the input optical beam into a high-frequency electric signal. The output voltage of the photodetector is linearly proportional to the E-field of the device under test. Because of the extremely small values of Pockels coefficients, the output voltage of the photodetector is very weak and often buried under the system's noise floor. An ultra-wideband multi-stage low-noise amplifier (LNA) is used to amplify this signal to a measurable level. In a frequency-domain near-field measurement configuration as shown in Fig. 1B, the amplified RF signal at the output of the photodetector is mixed with a local oscillator (LO) and is down-converted to an intermediate frequency (IF) of 100 MHz. Then a lock-in amplifier is utilized to measure both the amplitude and phase of this low-frequency signal, whose amplitude is directly proportional to the field strength of the device under test. A BSO probe with a <100> crystal cut can measure the normal component of the E-field of the DUT, while a BSO probe with a <110> crystal cut can measure the tangential E-field component.

The EO E-field probe is made of all dielectric materials with no metallic components and can be brought to the very-near-field region of the DUT in a minimally-distorting manner. Due to its relatively small footprint (1 mm^2), it can be used to measure the E-fields with high spatial resolution with minimal distortion to incumbent EM waves. The minimum sampled space can be less than 10 μm corresponding to the focused laser beam spot size within the EO crystal. Another advantage of the EO probe is its extremely wide bandwidth (1 kHz–40 GHz or higher). The lower limit of 1 KHz is due to the (1/f) flicker noise of the semiconductor laser source. As a result, heightened levels of both intensity noise and phase noise are generated at lower frequencies. This limits the ability to produce reliable polarization state modulation of the laser beam in the electro-optic crystal. The higher limit of 40 GHz is due to the high-frequency limit of the photodetector that is currently used in the NeoScan system. An ongoing research effort aims to push this limit to 100 GHz. We have studied the frequency response of the system by measuring calibration curves (for measurement in air) at various applied frequencies (spanning over 500 MHz to 40 GHz) all showing a linear relationship between the applied power and the measured signal strength (Supp. Fig. 1 and in a formerly published report for 40 GHz (Sarabandi et al., 2017)).

The probe can be calibrated to measure the absolute magnitude of E-fields over a wide dynamic range (0.1 V/m–1 MV/m). The sensitivity of the EO probes, in general, depends on the Pockels coefficient of the EO crystal. We are using BSO crystal, with a relatively high Pockels coefficient, because their high thermal stability. Lithium Titanium Oxide (LTO) crystals have a higher Pockels coefficient, but they are very sensitive to temperature changes. Our probes have been demonstrated to measure the absolute magnitude of E-fields as low as 1V/m incident field (Supp. Fig. 1). These curves are obtained when using a Lock-in amplifier in the system. To measure lower E-fields like 0.1 V/m, a high dynamic range spectrum analyzer should be used.

2.2. E-field probe calibration for measurement in biological tissue

In the measurement system for our EO probes, the output signal power, which is measured using either a spectrum analyzer or a lock-in amplifier, is proportional to the square of the E-field inside the BSO crystal:

$$P_{out} \propto |E_c|^2 \quad \text{(Eq. 1)}$$

where P_{out} (W) and E_c ($V.m^{-1}$) are the measured power by the system and the E-field inside the crystal, respectively. Therefore, for every power value measured by the system, the E-field inside the crystal is given by:

$$|E_c| = \alpha_1 . \sqrt{P_{out}} \quad \text{(Eq. 2)}$$

where α_1 ($V.m^{-1}.\ W^{-1/2}$) is a constant defined as the crystal to output calibration factor. Its value depends on the electronic attenuation of the system, BSO dimensions, and gain of the LNA.

The value of the E-field inside the crystal depends not only on the incident E-field that the probe is exposed to, but also on the physical characteristics of the surrounding medium (or more precisely the interface between the medium and the sensor's crystal). In other words, the E-field inside the crystal differs from the E-field inside the medium, in which it is placed in, due to the changes in dielectric properties at the interface of the medium material and the crystal. Therefore, the measurement system should be calibrated for the usage of each probe for application in a given medium (including air).

When the probe is placed inside a medium with a relatively homogenous distribution of E-field (which is the case for the situation where the dimensions of the probe is smaller than the wavelength in the medium), the induced E-field inside the crystal is scaled to the E-field in the medium (Supp. Fig. 2C–2D , and Jarrige et al., 2012) by:

$$|E_{med}| = \alpha_{2,med} . |E_c| = \alpha_1 . \alpha_{2,med} . \sqrt{P_{out}} = \alpha_{med} . \sqrt{P_{out}} \quad \text{(Eq. 3)}$$

where E_{med} ($V.m^{-1}$), $\alpha_{2,med}$ (a.u.) are the E-field in the medium surrounding the probe and a constant defined as the medium to crystal calibration factor, respectively. $\alpha_{med} = \alpha_1 . \alpha_{2,med}$ ($V.m^{-1}.\ W^{-1/2}$) is the total calibration factor of the probe, a medium-specific constant.

Each probe needs to be calibrated separately (i.e. its α_{med} should be determined) for application in a given medium. EO probes in air were calibrated using a known E-field in an air background such as the field inside a Transverse Electro Magnetic (TEM) cell antenna when excited with known RF power. For calibration of the probe inside a medium other than air, experiments containing such medium, with known dielectric properties and the values of the true E-field is required. For this purpose, similar to previous reports (Jarrige et al., 2012), we used a reservoir of the medium of interest inside a TEM cell (Supp. Fig. 3). For a given input power into the TEM cell, we calculate the E-field in the center of the reservoir via temperature measurements. It should be noted that the reservoir dimensions were verified in simulations (Fig. 2) to be sufficiently large for ensuring a homogeneous E-field in the location of the probe (i.e., center of TEM cell).

The EO probes that we used in our experiments (shown in Fig. 2A) have a directional preference, *i.e.,* they are sensitive to the *in-situ* E-field only from one direction and come in two formats: *normal probes* which are sensitive to the E-field parallel to the main axis of the probe, and *tangential probes* which are sensitive to the E-field at one direction in the plane perpendicular to the main axis of the probe (Fig. 2B). Because E-field in center of the cavities of a TEM cell is maximal in the direction perpendicular to the surface of its plates and minimal in other directions, two separate configurations of EO placement with regard to the TEM cell were used to calibrate different probe type (normal and tangential; Fig. 2C), leading to two calibration factors for the normal and tangential probes, respectively.

For the calibration method to work, an induced E-field in the medium, generated by the TEM cell, should be dominated by a single E-field polarization (*i.e.* perpendicular to the TEM cell's plates, Z in Fig. 2D), rather than in the other directions (X and Y in Fig. 2D). We validated this by numerical simulations as illustrated in Fig. 2D. As shown in this figure, the E-field along Z direction is > 10x higher than along the X- and Y-directions.

Fig. 2C shows the experimental set-up preparation for calibration of our normal and tangential EO probes. In order to calibrate our probes for E-field measurement in mouse brain, mice brains were extracted from healthy animals that were assigned to be sacrificed at the end of the experiments they were assigned to, collected from several laboratories in our institute. This prevented sacrificing the life of additional animals for the purpose of this experiment. Brain extraction was performed as close in time as possible to the experiment (one day before) and brain samples were kept in saline at 4 °C. Right before the experiment, we

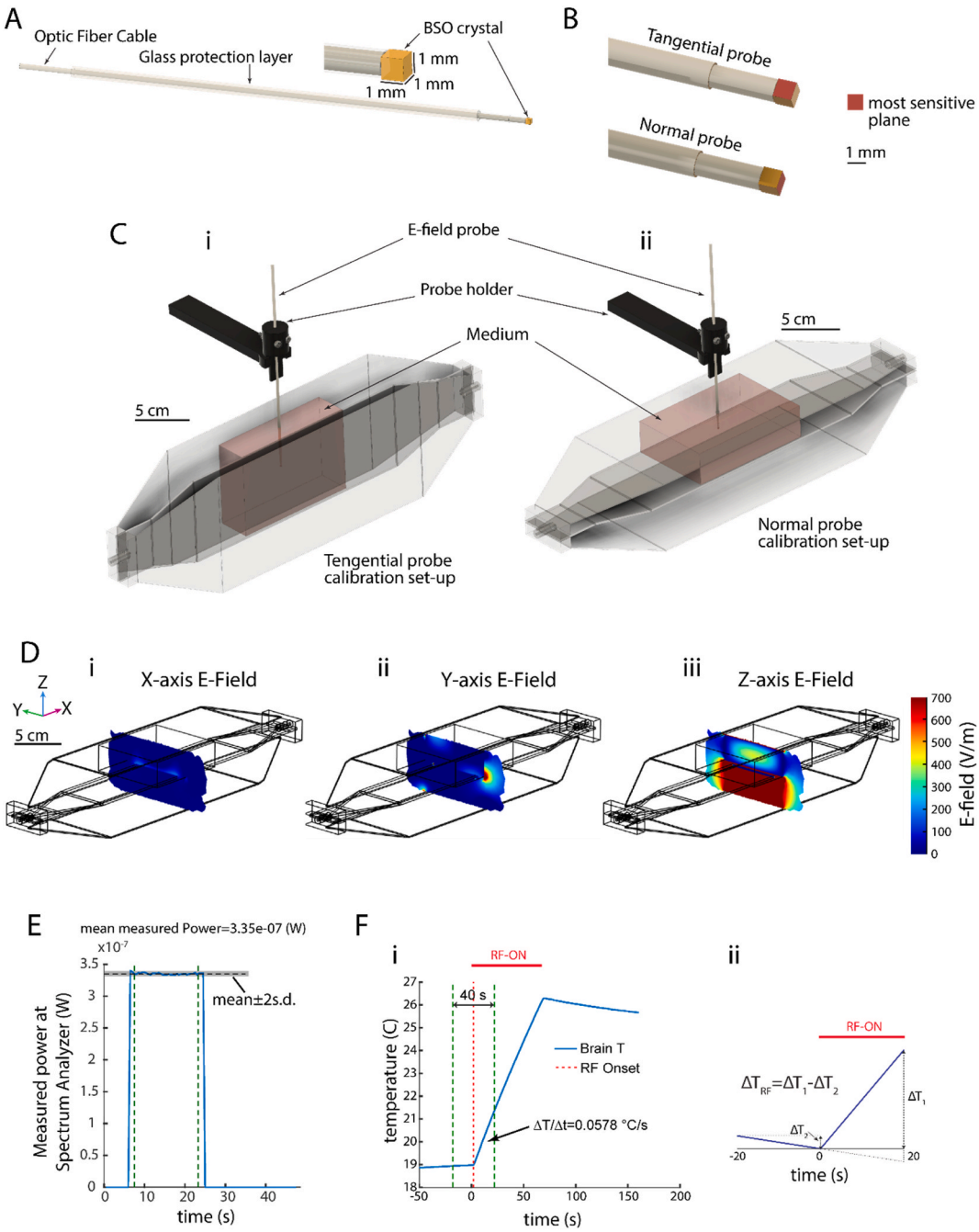

Fig. 2. Calibration of electrooptic E-field probes for measurements in a medium. A) Schematic of the E-field probe used in these experiments with a cubic (1 mm (Michaelson and Lin, 1987)) BSO crystal sensor. **B)** Schematic showing the sensitive plane on different probe types (tangential and normal). **C)** 3D schematic of the calibration set-up configuration for tangential (*left*) and normal (*right*) probes. E-field probe is placed in the center of a reservoir filled with the medium of interest (e.g., brain tissue) and placed at the middle of one of TEM cell's chambers. **D)** Numerical simulations, at 950 MHz, (COMSOL Metaphysics software) demonstrate that the E-field along the axis perpendicular to the TEM cell's septum (E_z) is an order of magnitude higher than in other directions (E_x and E_y). **E)** Example measurement curve showing non-calibrated power from the spectrum analyzer (measurement at 950 MHz). **F)** *i*: Temperature measurement using an optical temperature probe performed using the same set-up configuration as in C-*left*. *ii*: A simple plot showing how ΔT is calculated considering the slope of the temperature changes during the baseline.

removed the saline and made mixture of all brains. We filled the reservoir of our calibration set-up with this mixture and performed the probe calibration as discussed. Fig. 2E shows an example measurement (output power from the spectrum analyzer of the system) from a probe calibration experiment.

In order to calibrate the output of the system in each measurement, one needs to verify the value of the actual E-field at the probe's location (See Materials and Methods). Therefore, we conducted temperature measurements using an optical temperature probe (0.3 mm diameter, PRB-329 100-01M-STM, Osensa Innovation Corp.) to measure the rate of the induced temperature increase and the corresponding Specific Absorption Rate (SAR) and consequently the magnitude of the E-field. We conducted these temperature measurements in the configuration for calibration of the tangential probe as shown in Fig. 2Ci. The result was also used for the calibration of the normal probe also as the temperature measurement is sensitive to the magnitude of the total E-field and not to

its direction. Fig. 2Fi shows the change in temperature of the center of the brain mixture reservoir due to 70s of continuous-wave RF exposure (36W input power into the TEM cell). The resulting rate of T rise ($\Delta T/\Delta t$) calculated by considering 20s before and after the onset of the RF exposure (Fig. 2Fi) is 0.0578 °C/s which leads to a calculated SAR and E-field values of 204.45 W/kg and 617.64 V/m, respectively (see Materials and Methods, and Alon et al., 2016). During this short period after the onset of heating, heat removal from the system as well as heat diffusion across the brain is expected to be minimal, thus introducing small errors in the E field calculations. This statement is congruent with the linear temperature change observed in the brain at these heating time scales and intensities.

Dividing the un-calibrated measured power values (P_{out}) obtained from the calibration experiments (1.13e-6 W and 3.28e-7 W for tangential and normal probe (average from three repetitions), respectively) by the actual E-field strength deducted from the temperature measurements the calibration factor (defined as $\alpha_{calibration} = \alpha_{brain} = \alpha_1.\alpha_{2,brain} = |E_{brain}|/\sqrt{P_{out}}$ where E_{brain} (V.m^{-1}) is the actual E-field value in the center of reservoir filled with the brain tissue) for the tangential and normal probes used in our experiments were 5.81e5 (V.m^{-1}. W$^{-1/2}$) and 1.08e6 (V.m^{-1}. W$^{-1/2}$), respectively. These factors will be used to adjust the E-field reading in the in vivo experiments (as shown in Fig. 3).

In order to establish a simpler way for calibrating our EO probes without the need to sacrifice a large number of animals, we examined our methodology on a phantom material with similar physical characteristics compared to the mice brain tissue. We developed a simple method to produce such phantom material from commercially available products (see Materials and Methods). We used a similar approach as

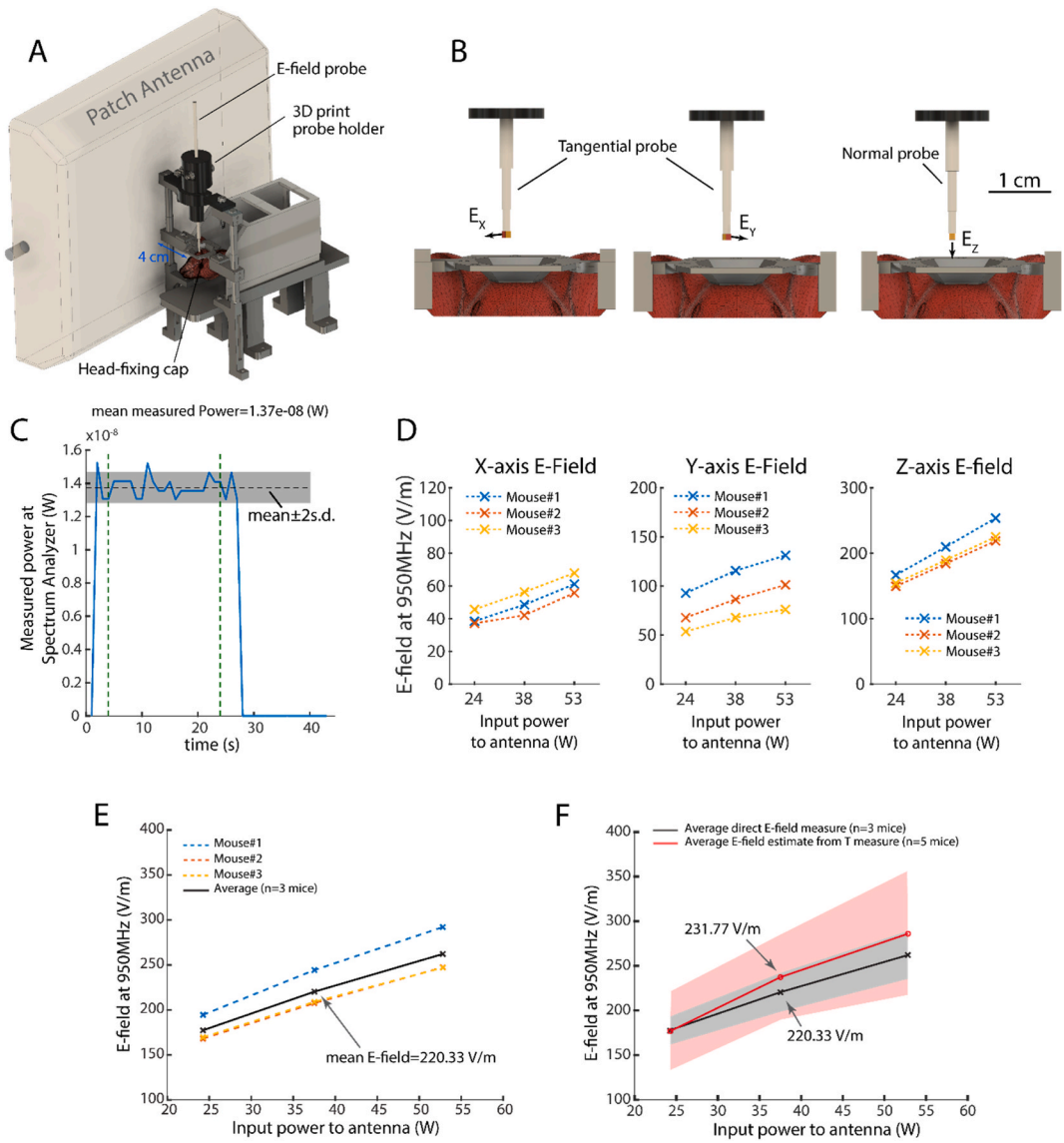

Fig. 3. Direct measurement of E-field magnitude in mice brains *in-vivo*. A) Schematic of the experiment set-up: a mouse implanted with the EO probe is head-fixed and a patch antenna is placed next to the animal in a fixed position (4 cm away from animal's head). **B)** illustration of the measurement procedure to obtain E-fields along the x-,y-, and z-orientations. From left to right: first a tangential probe is implanted and E-field measurement is performed. Then the probe is extracted from the brain (but remains in the set-up) and turned 90° on the plane parallel to surface of the skull. The probe is implanted back in the brain and E-field is measured. Finally, the tangential probe is completely removed from the setup and a normal probe is implanted, and E-field is measured. **C)** Example curve showing non-calibrated power from the spectrum analyzer for in-vivo Y-axis measurement for 38W RF input power to antenna. **D)** Calibrated E-field magnitude values measured along the three axis shown in B (n = 3 mice). **E)** Total E-field magnitude (n = 3 mice) using data in D. **F)** Comparison between the E-field values obtained by direct measurement of E-field using EO probes (this study) and values estimated from in-vivo temperature measurements (mean (line) ± standard deviation (shaded area)).

that of probe calibration in brain tissue using temperature measurements. Supp. Fig. 4 shows the change in temperature of the center of the phantom material reservoir due to 70s of continuous-wave RF exposure (36W input power into the TEM cell). The resulting rate of T rise ($\Delta T/\Delta t$) calculated by considering 20s before and after the onset of the RF exposure is 0.0373 °C/s which leads to a calculated SAR and E-field values of 168.15 W/kg and 625.90 V/m, respectively (see Materials and Methods, and Alon et al., 2016). The power values (P_{out}) measured in the calibration experiment with the phantom material were 9.80e-7 W and 2.67e-7 W for tangential and normal probe, respectively. As the phantom material we made has a high viscosity, it is possible to use temperature measurement to estimate the E-field. This is validated by comparing the calibration results with calibration coefficients of 6.32e5 ($V.m^{-1}.\ W^{-1/2}$) and 1.21e6 ($V.m^{-1}.\ W^{-1/2}$) for the tangential and the normal probes, respectively whose difference with the values obtained using the brain tissue sample are 8.8% and 12.3%, respectively.

2.3. Numerical simulations to assess the effects of material properties on the E-field measurement

We performed finite-element numerical simulations to study the effects of electrical conductivity (σ) and relative permittivity (ε_r) of the medium on the induced E-field inside the crystal and consequently on the measurement. We created a 3D model of the experimental setup of the probe calibration procedure presented in Fig. 2C. We conducted simulation runs, using COMSOL Multiphysics software (Comsol Inc.), with parametric sweeps for σ, varying its value from 0.4 to 4 ($S.m^{-1}$) with 0.2 ($S.m^{-1}$) incremental steps and for ε_r, varying its value from 1 to 78.5 with 2.5 incremental steps. Supp. Fig. 2A shows the 3D design of the experiment in COMSOL. Supp. Fig. 2B illustrates the probe configuration used in the simulation including numerical probing volumes to measure the E-field at the center of the BSO crystal and at its adjacent volumes in the medium of interest. Supp. Fig. 2C–2D confirm a linear relationship between the measured E-field (in any of the probing volumes) and the square root of the input power to the TEM cell and between any pair of the measured electric-field values for a given input power. As the EO probe output depends on the ratio between the E-field in the center of the crystal and the E-field at its neighboring medium (at its bottom for the normal probe and at one of its lateral sides for the tangential probe), we next examined this ratio as a function of relative permittivity (Supp. Fig. 2E) and electrical conductivity (Supp. Fig. 2F) of the medium for a fixed input voltage, hence a fixed input power (here 36 W, similar to our probe calibration experiments) to the TEM cell, and in the case of a normal probe as an example. Note the relatively low variability of the measured ratio between the E-field values when either the relative permittivity or the electrical conductivity of the medium is set close to those corresponding to the brain tissue (57 and 1 S/m, respectively) and the other one is varying. This shows that calibrating the EO probes using a phantom with a relative permittivity and an electrical conductivity close to same parameters in the brain tissue constitute a reliable methodology.

One important outcome from these simulations is that the medium-specific calibration coefficients depend on the electrical conductivity and the relative permittivity of the medium which themselves are frequency-dependent. Therefore, every probe should be calibrated for the specific frequency of the experiment prior to the measurements in a given medium.

2.4. Direct measurement of RF E-field in mice brains in-vivo

We conducted experiments to measure *in-situ* E-field magnitude in the brain of urethane-anesthetized mice. We head-fixed the mice to ensure a similar RF E-field exposure for all experiment repetitions. We replicated the set-up from one of our recent studies where the effect of RF exposure on neuronal activity monitored by 1-photon Ca^{2+} imaging in-vivo was investigated (Yaghmazadeh et al., 2022). As part of that study, we performed numerical simulations to evaluate the field distribution in a realistic mouse model placed in an exact representation of the experimental set-up (Yaghmazadeh et al., 2022). As it can be seen in that report the E-field distribution in the brain is relatively homogenous, showing that the presence of the skin and skull does not disturb the field in a manner to affect the E-field measurement.

Fig. 3A shows the experimental set-up for the head-fixed mouse with implanted EO probe in the brain. We measured the E-field values from three orthogonal directions using a normal and a tangential EO probe. As illustrated in Fig. 3B we first implanted the tangential EO probe and measured the E-field along the x axis (E_x). Then, we extracted the tangential probe and rotated it for 90°, implanted it to the same depth in the brain and measured the E-field along the y axis (E_y). Next, the tangential probe was extracted from the brain and replaced it with the normal probe which was then implanted to the same coordinates inside the brain and E-field along the z axis (E_z) was recorded. Fig. 3D and E shows the results of the measurement of the magnitude of E-field along different directions (E_x, E_y, and E_z) and the total E-field (E_{tot}, see Materials and Methods). These results are calculated using the calibration coefficients obtained in probe calibration experiments in brain tissue.

As shown in Fig. 3F, the in-vivo E-field measurement results obtained in this study are in good agreement with the E-field values driven from in-vivo temperature measurements (see Materials and Methods and Supp. Fig. 5) performed by an optical temperature probe (1.1 mm diameter, OTP-M, Opsens Solutions Inc.).

3. Discussions

This manuscript demonstrates direct measurement of E-field magnitude, using BSO crystal based EO probes, in mice brain *in-vivo*. We introduced a novel method for *in-vivo* measurement of E-field in biological tissue, enabling accurate dosimetry studies in exact experimental scenarios.

This study presents an unprecedented demonstration of measurement of RF electric fields in the live tissue. Our approach opens a path towards direct measurement of E-fields in-vivo for precise RF dosimetry, historically performed numerically or in phantom preparations. Our method also provides the opportunity to fine-tune indirect dosimetry approaches. This is particularly of high importance given the growing concerns on the effect of RF energy radiation on health and environment enhanced by development of novel technologies and applications.

3.1. Medium preparation for calibration process

To calibrate our EO probes for E-field measurements in mice brain, we prepared a mixture of brain tissue extracted from several animals. It is possible that the dielectric properties of the ex-vivo brain does not match the *in-vivo* brain. Yet, extracting the brain samples close to the experiment time and keeping them in saline at 4 °C kept the tissue as fresh as possible and the physical properties of the resulting sample remains as close as possible to those of the brain (See dielectric measurement description in the Materials and Methods section). Nevertheless, the results obtained were in good agreement with E-field values computed from the temperature control experiments (Fig. 3F) and potential errors in the calibration process, including medium preparation, did not induce an error beyond the already existing cross-animal measurement variabilities (which we also observed in our temperature control experiments). Development of novel probe structures with established physics-based analytical expressions for effects of surrounding medium on induced E-field inside the probe could remove the need for calibration in brain tissue. For example, the E-fields inside a spherical object immersed in a background medium can be expressed by Rayleigh's theory (Bohren and Huffman, 1998). Such new generation of probes could be calibrated by prepared material samples for measurement in any medium, and be used in different medium, provided that the physical properties are known.

3.2. Prominent applications

Our experiments, demonstrating direct measurement of RF E-fields *in-vivo*, introduce a framework that can be used and further developed for different applications, such as: 1) non-distorting measurement of RF E-Field: metal-inclusive probed are invasive to the distribution of the field they are immersed in. EO probes provide the possibility of minimally-distorting direct measurement of the RF E-field and our study demonstrates the feasibility of their *in-vivo* application which can be employed in the following applications: a) MRI and RF safety dosimetry in animal models and in biological tissue or phantoms: *in-vivo* measurements in animals can be used for direct and accurate safety measurements but also to examine and fine-tune simulations. b) Dosimetry in proximity of medical implants: one of the main safety concerns about RF applications (such as MRI, inspection devices, RF equipment, etc.) is the potential danger for people and patients with metallic implants. Animal models can be used to study such effects in live tissue rather than current approaches relying on *ex-vivo*, phantom or simulation studies. In this regard, using EO probe technology can be highly desirable given the fact that these probes minimally interact with the EM field. 2) low power dosimetry: Optical temperature measurements have also been shown to be a suitable way to provide an indirect estimate of the E-fields, but their application is reliable only for higher level of RF power where adequate temperature change is induced in the tissue. EO probes are the appropriate choice for measurements of the electric field induced by low power RF energy in the tissue.

3.3. Uncertainties and improvements

The results of our measurements demonstrate a noticeable extent of variability. We attribute this variability to various parameters including: 1) animal to animal difference: variability in age, body and head size, tissue (skin, fat, etc) between animals lead to an extended distribution of the induced E-field at the point of measurement. 2) Probe replacement: due to the three-step measurement procedure (Fig. 3B), the impact of the error of misplacement of the probe is increased. Development of three-axial probes can reduce this error. 3) Probe size versus mouse head volume: although probe dimensions in this set of experiments are small enough to allow implanting *in-vivo* and obtain relatively accurate measurements, the 1 mm size of the probe adds some variability on the measurement from one animal to other. Development of sub-millimeter probes can help reduce this effect. 4) Dielectric and thermal property estimation: both experiments and simulations utilized information about the media in order to estimate the electric field (either by calibrating in phantoms with known thermal and dielectric properties, or via conduction of E-field simulations). A >10% uncertainty in the estimation of both the thermal and dielectric properties of the brain tissue has been reported in past studies (Sasaki et al., 2022) and is incumbent on this study as well. With these uncertainties in mind the E-field measurements exhibited an inter-animal variability of 16.3%. These errors are generally low, as for example in cellphone compliance testing conducted in phantoms, the maximum allotted errors are on the order of 30% (Marinescu, 2008). In addition, the dielectric properties of different brain tissue types (white matter, grey matter and the cerebrospinal fluid) are varying, making dosimetry experiments challenging. This is even more important in rodents as the dimensions of different brain regions (with different dielectric properties) are very small (in comparison to available probes). As also suggested by former reports (Steel and Sheppard, 1985) one way to deal with this variability is to use dielectric values that represent the 'average' brain tissue. As it is shown in the same report macerated brain, which is prepared in a very similar way to how we made our brain mixture medium, is indeed behaving as such 'average' brain tissue over a wide range of frequency (from 1 GHz to 18 GHz). Development of next generation of E-Field probes with much smaller footprint would help overcome this challenge.

While our experiments successfully demonstrate the possibility of direct measurement of RF E-fields *in-vivo*, further developments for improving the E-Field probes can ameliorate the quality and accuracy of the measurement. Some of such potential improvements include: 1) the development of a 3-axis probe that would reduce variability in (re)implantation and measurement procedure; 2) smaller probe footprint, enabling smaller field perturbation and leading to more accurate E-field readings with a decrease in tissue damage; 3) integration of EO E-field and optical temperature measurement: such technology would allow self-calibration of E-field values with temperature change measured at the same location in space.

3.4. Future directions

Using realistic numerical animal models, obtained from imaging experiments, with precise anatomical reproduction of the tissue, one can perform simulations to assess E-field values in the brain and compare the outcome with the presented results in this paper. Such study would provide a framework for calibration of in-silico evaluation of RF dosimetry based on direct measurements in-vivo.

A real-life scenario experimental application of the presented method consists of measurement of E-field in the brain of rodents while exposed to a nearby cell phone in different conditions (during a call, surfing the internet or standby). Such experiment would provide precise dosimetry results to be compared with previous reports and the safety guidelines for RF applications. Today cell phone applications (including 3G, 4G LTE and 5G technologies) use frequencies spanning from few hundreds of MHz to up to several tens of GHz (in the case of 'high band 5G'). For example, in the united states the occupied frequencies expand over 600Mhz-39GHz range across different service provides. All these frequencies are covered by the present development of NeoScan system.

Another extension of this work can be conducted for direct and accurate measurement of RF E-fields in HPM applications. HPM applications, covering both civil and military usage, are defined as high peak power bursts of narrowband RF radiation spanning the frequency range of approximately 1 GHz–100 GHz (Schamiloglu, 2004). Most applications are however developed at frequencies ranging from ~1 GHz to 40 GHz (Guoqi et al., 2005). While this frequency range is covered by present development of the NeoScan system, there is ongoing development to cover as high as 100 GHz in the near future.

Finally, other application can include direct E-field measurement at higher frequencies such as millimeter-waves, where RF energy is absorbed in shallow depths (given the skin-effect) and related studies on in-vivo dosimetry are of high interest in the research field.

4. Materials and methods

4.1. Experiments

4.1.1. Phantom material preparation

We mixed the following materials in mass proportion until a homogenous solution was obtained: 130 gr (or 0.64% mass ratio) Corn Syrup (Golden, King Syrup, USA), 70 gr (or 0.35% mass ratio) Distilled water, 2 gr (or 1% mass ratio) salt (NaCl). The density (ρ), relative permittivity (ε), electrical conductivity (σ) and heat capacitance (C) were measured giving 1233.23 (Kg/m^3), 47.84 at 950 MHz, 1.06 (S/m) at 950 MHz and 4514.17 (J/Kg.°C), respectively. Relative permittivity and electrical conductivity were measured using a dielectric probe kit (85070 E, Agilent Tech. Inc.) and heat capacitance was measured using a KD2 thermal properties analyzer (Decagon Devices Inc.).

4.1.2. Brain tissue preparation

We collected 219 mice, different types both male and female, from various laboratories in our institution, that were on the waiting list to be sacrificed, mostly because they were untagged animals from breeding of genetically modified mice lines. This approach avoided purchasing and killing extra animals. Mice were kept in cages in a 12hr regular cycle

vivarium room dedicated to mice in up to five-occupancy cages. No prior experimentation had been performed on the animals. Mice were sacrificed the day before the probe calibration experiment and their brains were extracted. Brain were kept in saline at 4 °C overnight. Prior to the experiment saline was extracted and brain tissue were mixed. We measured the following physical properties of the brain tissue mixture: density (ρ), relative permittivity (ε), electrical conductivity (σ) and heat capacitance (C) and obtained 988.93 (Kg/m^3), 57.77 at 950Mhz, 1.06 (S/m) at 950 MHz and 3540 (J/Kg.°C), respectively. Relative permittivity and electrical conductivity were measured using a dielectric probe kit (85070 E, Agilent Tech. Inc.) and heat capacitance was measured using a KD2 thermal properties analyzer (Decagon Devices Inc.).

4.1.3. Sensor calibration for E-field measurement in a medium

For calibration of the EO E-field probes, we positioned them at the center of a reservoir filled with the medium of interest that we placed in the middle of one of the two chambers of a TEM cell antenna (TBTC0, Tekbox Digital Solutions). A specific set-up configuration was used for calibration of tangential or normal probes as shown in Fig. 2C. The TEM cell was fed with RF energy generated by a signal generator (845–26, BNC Berkeley Nucleonic) and an amplifier (ZHL-100W-13+, Mini-circuits). After setting-up the experiment configuration, RF energy was injected into the TEM cell (36W input power) and uncalibrated E-field value was recorded using the E-field measurement system (NeoScan, EMAG Tech. Inc) for at least 20s (1Hz sample rate). The E-field probe was then removed and replaced by an optical temperature probe (0.3 mm diameter, PRB-329 100-01M-STM, Osensa Innovation Corp.) in the same position, where temperature was recorded for 50s of baseline (no RF energy applied) followed by 70s of RF energy application into the TEM cell (36W input power). RF power was monitored using a power meter (U2001A Power Sensor and N9912A Field Fox Spectrum analyzer, Agilent/Keysight) that measured the forward and reflected power on a bidirectional coupler (778D, Agilent/Keysight) that was in line with the transmit chain.

4.1.4. Numerical simulations

A 3D implementation of our probe calibration set-up, consisting of a TEM cell antenna with a reservoir filled with a medium of interest placed in the middle of one of its chambers, was created in COMSOL Multiphysics software (Comsol Inc.). A 3D EO probe, consisting of a 1 mm^3 cubic BSO crystal attached to a cylindrical glass optic-fiber, was placed at the same location as in our probe calibration experiment for the normal probe. We defined virtual probing volumes at the center of the BSO crystal and adjacent to its bottom and lateral walls to monitor the E-field (measured as average over the volume) at different locations. First, simulations were conducted with a parametric sweep on the input voltage (and hence the input power) of the TEM cell. Then, at a fixed input power to the TEM cell (36W as in our probe calibration experiments) we performed a 2D parametric sweep, where the relative permittivity was changed from 1 to 78.5 with 2.5 increments and the electrical conductivity was changed from 0.4 to 4 (S.m^{-1}) with 0.2 (S.m^{-1}) increments, to evaluate the effects of the dielectric properties of the medium on the E-field sensing of the EO probe. Results of E-field virtual probing volumes were plotted following completion of the simulations.

4.1.5. Animals for the in-vivo E-field measurements

Adult wild-type male C57BL/6JxFVB mice (20–24 gr) were obtained from Charles River Laboratory. Mice were kept in cages in a 12hr regular cycle vivarium room dedicated to mice in up to five-occupancy cages. In all experiments, each animal served as its own control, no randomization or blinding was employed. No prior experimentation had been performed on the animals. All experiments were conducted in accordance with the Institutional Animal Care and Use Committee (IACUC) of New York University Medical Center.

4.1.6. EO E-field probe implantation and in-vivo RF E-field measurement

The implantation surgery was performed in two separate steps. Two days before the experiment, mice were anesthetized by isoflurane and a head-cap base matching the head-fixing set-up was attached to their skulls. In the day of the experiment, mice were anesthetized by urethane (1.5 g/kg, intraperitoneal injection) and positioned on the head-fixing set-up next to a stereotaxic system. A craniotomy was made and using the stereotaxic system the E Field probes were located inside the brain at a fixed location (similar to the location of the imaging lens in a former related experiment (Yaghmazadeh et al., 2022), at AP −2.1 mm, ML 1.5 mm, DV 1.5 mm coordinates from the Bregma point of the skull). The probes were secured by a custom-made 3D printed holder fixed to the head-fixing set-up (Fig. 3A). The set-up was then freed from the stereotaxic system and was moved to the adjacent room where the RF stimulation was performed. The patch antenna was placed 4 cm away from the animal's head (Fig. 3A) in the exact way as used in our former study (Yaghmazadeh et al., 2022). E-field measurement was done by two types of E-field probes: 1) normal probe which measures the E-field along the central axis of the probe and 2) tangential probe which measures the E-field along a certain direction perpendicular to the axis of the probe. To measure three orthogonal components of the E-field inside the brain the following process was used: First the tangential probe was implanted and the E Field along a direction perpendicular to the probes axis is measured (E_X). Then, the probe was taken out and turned 90° and E Field in a perpendicular direction relative to the first direction and to the axis of the probe was measured (E_Y). Finally, the tangential probe was taken out and the normal probe was implanted and the E-field along the axis of the probe was measured (E_Z). Note that E_X, E_Y, and E_Z are the measured values after applying their respective calibration factors for the corresponding E-field probes. The total E-field is expressed as ($E_{TOT} = E_X.\hat{x} + E_Y.\hat{y} + E_Z.\hat{z}$) with a magnitude computed according to ($|E_{TOT}| = \sqrt{E_X{}^2 + E_Y{}^2 + E_Z{}^2}$). Animals were humanely euthanized at the end of the experiment.

4.2. Analysis

4.2.1. Calculation of SAR and E-field from temperature measurements

Temperature changes induced by continuous-wave RF exposure (Fig. 2F) was used to calculate SAR and E-field values using

$$\rho C\frac{dT}{dt} = \nabla.(k\nabla T) + SAR\rho \quad \text{(Eq. 4)}$$

where ρ is the tissue density (kg/m3), C is heat capacity (J/kg/C), k is thermal conductivity (W/m/C), and SAR (W/kg) is the driving force for temperature rise defined as: $SAR = \sigma|E|^2/2\rho$ (Eq. 5), where E is the induced E-field (V/m), and σ is the electrical conductivity (S/m). Under the short-term heating regime, Eq. (4) is simplified to: $SAR = C\Delta T/\Delta t$ (Eq. 6) where ΔT/Δt is the temporal rate of temperature increase. Therefore, knowledge of the dielectric properties and thermal properties of the tissue, and heating duration (measured as specified above), as well as the temperature changes can effectively be used to estimate the magnitude of the electric field, provided it is dominated by a single polarization. SAR was calculated from the temporal temperature increase rate using Eq. 6 and E-field was driven from SAR values using Eq. 5 ([19]).

CRediT authorship contribution statement

Omid Yaghmazadeh: Conceptualization, Methodology, Validation, Formal analysis, Investigation, Data curation, Visualization, Supervision, Project administration, Funding acquisition, Writing – original draft, Writing – review & editing. **Seth Schoenhardt:** Investigation. **Arya Sarabandi:** Investigation. **Ali Sabet:** Investigation. **Kazem Sabet:** Writing – original draft, Resources. **Fatemeh Safari:** Investigation. **Leeor Alon:** Investigation, Resources, Formal analysis, Writing – review

& editing. **György Buzsáki:** Funding acquisition, Conceptualization, Resources, Writing – review & editing.

Declaration of competing interest

The authors declare the following financial interests/personal relationships which may be considered as potential competing interests: Seth Schoenhardt, Arya Sarabandi, Ali Sabet, Kazem Sabet reports a relationship with Emag Technologies Inc that includes: employment.

Data availability

Data will be made available on request.

Acknowledgements:

Authors thank Mihaly Voroslakos for his help in the early establishment of this collaboration. O.Y. thanks Chiung-Yin Chung, Jingjing Liu, Pavan Veeramreddy, Riccardo Melani, Gergely Komlosi and Marisol Soula for their help with brain tissue preparation. This work was supported by the following grants: NIH-R01 (# 1R01NS113782-01A1) and NIH-TL1 postdoctoral fellowship (#2TL1TR001447-06A1) to O.Y.

Appendix A. Supplementary data

Supplementary data to this article can be found online at https://doi.org/10.1016/j.biosx.2023.100328.

References

Alon, L., Sodickson, D.K., Deniz, C.M., 2016. Heat equation inversion framework for average SAR calculation from magnetic resonance thermal imaging. Biolectromagnetics 176, 139–148.

Bohren, C.F., Huffman, D.R., 1998. Absorption and scattering by a shpere. In: *Absorption And Scattering of Light by Small Particles* 82–129. WILEY-VCH Verlag GmbH & Co. KGaA.

Cecelja, F., Balachandran, W., 1999. Electrooptic sensor for near-field measurement. IEEE Trans. Instrum. Meas. 48, 650–653.

Dagro, A.M., Wilkerson, J.W., Thomas, T.P., Kalinosky, B.T., Payne, J.A., 2021. Computational modeling investigation of pulsed high peak power microwaves and the potential for traumatic brain injury. Sci. Adv. 7, 1–11.

Daily, L.E., 1943. A clinical study of the results of exposure of laboratory personnel to radar and high frequency radio. Nav. Med. Bull. 41, 1052.

Faraone, A., McCoy, D.O., Chou, C.K., Balzano, Q., 2000. Characterization of miniaturized E-field probes for SAR measurements. IEEE Int. Symp. Electromagn. Compat. 2, 749–754.

Follis, R.H., 1946. Studies on the biological effect of high frequency radio waves (radar). Am. J. Physiol. 147, 281.

Foster, K.R., 2000. Thermal and nonthermal mechanisms of interaction of radio-frequency energy with biological systems. IEEE Trans. Plasma Sci. 28, 15–23.

Gabriel, C., Gabriel, S., 1996. Compilation of the Dielectric Properties of Body Tissues at RF and Microwave Frequencies.

Gabriel, C., Gabriel, S., Corthout, E., 1996. The dielectric properties of biological tissues: I. Literature survey. Phys. Med. Biol. 41, 2231–2249.

Guoqi, N., Benqing, G., Junwei, L., 2005. Research on high power microwave weapons. Asia-Pacific Microw. Conf. Proceedings, APMC 2.

Jarrige, P., et al., 2012. Electrooptic probe adapted for bioelectromagnetic experimental investigations. IEEE Trans. Instrum. Meas. 61, 2051–2058.

Karipidis, K., Mate, R., Urban, D., Tinker, R., Wood, A., 2021. 5G mobile networks and health—a state-of-the-science review of the research into low-level RF fields above 6 GHz. J. Expo. Sci. Environ. Epidemiol. 31, 585–605.

Keiber, S., et al., 2016. Electro-optic sampling of near-infrared waveforms. Nat. Photonics 10, 159–162.

Marinescu, A., 2008. Measurement uncertainty at SAR determination for mobile phones. In: The 6th International Symposium on ADVANCED TOPICS IN ELECTRICAL ENGINEERING, pp. 1–5.

Michaelson, S.M., Lin, J.C., 1987. Biological Effects and Health Implications of Radiofrequency Radiation. Plenum Press.

Sarabandi, K., Choi, J., Sabet, A., Sabet, K., 2017. Pattern and gain characterization using nonintrusive very-near-field electro-optical measurements over arbitrary closed surfaces. IEEE Trans. Antenn. Propag. 65, 489–497.

Sasaki, K., Porter, E., Rashed, E.A., Farrugia, L., Schmid, G., 2022. Measurement and image-based estimation of dielectric properties of biological tissues —past, present, and future. Phys. Med. Biol. https://doi.org/10.1088/1361-6560/ac7b64.

Schamiloglu, E., 2004. High power microwave sources and applications. IEEE MTT-S Int. Microw. Symp. Dig. 2, 1001–1004.

Schuderer, J., Schmid, T., Urban, G., Samaras, T., Kuster, N., 2004. Novel high-resolution temperature probe for radiofrequency dosimetry. Phys. Med. Biol. 49.

Steel, M.C., Sheppard, R.J., 1985. Dielectric properties of mammalian brain tissue between 1 and 18 GHz. Phys. Med. Biol. 30, 621–630.

Sulzer, P., et al., 2020. Determination of the electric field and its Hilbert transform in femtosecond electro-optic sampling. Phys. Rev. 101, 1–17.

Vöröslakos, M., Yaghmazadeh, O., Alon, L., Sodickson, D.K., Buzsáki, G., 2022. Brain-implanted conductors amplify radiofrequency fields in rodents: advantages and risks. bioRxiv, 2022.07.20.500859. https://doi.org/10.1101/2022.07.20.500859.

Wu, Q.Z.X.-C., 1997. 7 terahertz broadband GaP electro-optic sensor. Appl. Phys. Lett. 70, 1784–1786.

Yaghmazadeh, O., et al., 2022. Neuronal activity under transcranial radio-frequency stimulation in metal-free rodent brains in-vivo. Commun. Eng. 1.

Ziegelberger, G., et al., 2020. Guidelines for limiting exposure to electromagnetic fields (100 kHz to 300 GHz). Health Phys. 118.